Coding for Circuit Integration in the Injured Brain by Transplanted Human Neurons

Zhifu Wang[1,3] *, Danyi Zheng[1,3], Shu-Min Chou[1], Phil Jun Kang[2], Fei Ye[1], Su-Chun Zhang[1,2,4,5]**
[1]Program in Neuroscience and Behavioral Disorders, Duke-NUS Medical School, Singapore
[2]Center for Neurologic Diseases, Sanford Burnham Prebys Medical Discovery Institute, La Jolla, CA, USA
[3]These authors contributed equally
[4]Senior author
[5]Lead contact
*Correspondence: wang.zhifu@duke-nus.edu.sg
**Correspondence: suchunz@sbpdiscovery.org

Highlights

Human ESC-derived cortical neurons reconstitute the ischemic motor cortex

Functionally repaired corticospinal tract restores animal behaviors

Transplanted cortical neurons exhibit subtype-specific projection and integration

Unique transcriptional coding for axonal navigation in the mature CNS

SUMMARY

Neural transplantation holds the potential to repair damaged neural circuits in neurological diseases. However, it remains unknown how the grafted neurons project axons to and make functional connections with the appropriate targets to repair the damaged circuit at the adult stage. Here we report that human cortical progenitors, transplanted into the ischemic mouse motor cortex, matured and integrated into cortical and subcortical neural circuits including the corticospinal tract. Neuronal tracing combined with single-nuclei RNA sequencing revealed the close relationship between the transcription profiles of a cortical neuronal subtype, especially those of axon guidance and synapse assembly, with the specific target projection and synapse organization. Machine learning-based regression further identified the transcriptional codes for the targeted projection and circuit integration to reconstruct the damaged circuits. Our finding opens a promising strategy for treating neurological diseases through promoting regeneration and neural transplantation.

INTRODUCTION

The human brain has a limited regenerative capacity. Transplantation of neural progenitor cells (NPCs) offers a promising approach to replace the lost neurons and reconnect the damaged circuits. Indeed, transplantation of NPCs derived from pluripotent stem cells, including human embryonic stem cells (hESCs) or induced pluripotent stem cells (hiPSCs), is now in clinical trials for Parkinson's disease (PD), epilepsy, and age-related macular degeneration. However, how the grafted neurons find and make functional connections with their targets in the mature injured brain remains unclear. This makes neural transplantation therapy less predictable, especially for diseases of the cerebral cortex that affect diverse neuronal subtypes and multiple neural circuits including the long-distance corticospinal tract (CST).

Cortical neurons or organoids transplanted into the postnatal brain exhibit low efficiency in extending axons from the neocortex to the brainstem[1], with even fewer projections observed when grafted into the brains of adult animals following traumatic brain injury or stroke[2,3]. Meanwhile, the injury leaves an open cavity surrounded by glial scars, resulting in a hostile microenvironment that severely limits the survival and integration of transplanted neurons, preventing effective structural repair and reconstruction of the damaged neural circuitry. Single cell profiling of retrogradely labelled neurons revealed the self-organized process during development based on the association between the transcriptome of cortical neuronal subtypes and their projection targets[4-6]. However, the injured brain environment at adult stage differs significantly from the developing brain in both structure and molecular composition, and circuit integration relies on a complex combination of guidance molecules[7]. Substantial numbers of graft-derived axons are often observed in stochastic, unrelated brain regions. Even the neurons originating from the visual cortex, transplanted into the visual cortex, project to the agranular insula, striatum, amygdala, and superior colliculus[8-10], only partly corresponding to the host neural circuits. On the other hand, hESC-derived midbrain dopaminergic (mDA) neurons, transplanted into the substantia nigra (SN), primarily grow axons along the medial forebrain bundle (MFB) to innervate the striatum[11,12], whereas cortical neurons transplanted into the SN project to the prefrontal cortex[11]. These phenomena suggest that the organization principle of the projection and connectivity in the damaged adult brain is different from the self-organizing processes observed during brain development[13]. Hence,

identifying the basic principle of pathfinding and circuit integration by grafted neurons in the mature brain will enable us to develop not only a predictable as well as safe and effective cell transplantation therapy but also regenerative therapy for brain disorders.

We reconstructed subcortical neuronal circuits, including the CST, in the ischemic stroke brain by transplanting subtype-specific deep-layer cortical neurons. These specific cortical neurons facilitated more efficient establishment of targeted projections and were sufficient to reconstruct long-distance neural circuits without overgrowth. This finding suggests a potential link between axonal projection directions and neuronal subtype identity. Single-nucleus RNA sequencing (snRNAseq), in combination with barcoded retrograde tracing, revealed that transplanted cortical neurons showed subtype-specific projection and integration. The subtypes of hPSC-derived cortical neurons, transplanted in the adult brain, possess distinct combinations of axon guidance and synaptic assembly molecules that are similar to but distinguishable from those required in endogenous human neurons. We further identified the transcriptional codes for specific projection and circuit integration in the mature brain with machine learning. These findings highlight the necessity of developing appropriate neural types for integration into target neural circuits in the injured brain by neural transplantation at the adult stage.

RESULTS

Transplanted human cortical neurons project to specific brain regions

The stroke cavity presents a hostile environment for transplanted cells; hence, grafting is typically performed in adjacent healthy brain regions instead[3,14-16], leaving the injured cortex open and unrepaired. We previously developed a cocktail that supports the survival of neural cells transplanted into the ischemic cavity[17]. To reconstitute the ischemic cortex and restore damaged circuits, we first differentiated hESCs into cortical NPCs for transplantation (Figure 1A). The cortical NPCs at day-35 contained over 70% progenitors expressing both CTIP2 and FEZF2 (markers of layer 5 pyramidal neurons) with less than 20% expressing layer-6 marker TBR1 (Figures 1B and S1A-S1B). The ischemic stroke models were induced by photothrombosis in the motor cortex of 12-week-old immunodeficient mice (Figure S1). The cortical NPCs were transplanted into the lesion cavity of ischemic stroke models (Figure S1). In total, we successfully performed cortical

neuron transplants in 95 mice (Supplementary Table 1). Twelve months post transplantation, the graft filled the stroke cavity with no overgrowth (Figures 1C and S1C).

Immunohistochemical analysis showed that 90% of transplanted cells expressed the neuronal marker NeuN (Figures 1D and 1E), indicating differentiation into neurons. About 63% of grafted cells were CTIP2^{+}/ FEZF2^{+}/ TBR1^{-} neurons (Figures 1F and 1G), consistent with the pre-transplantation cell population, suggesting that these cortical NPCs were cell fate-committed before transplantation. Single-nucleus RNA sequencing (snRNA-seq) revealed that the grafted human cells were predominantly deep layer neurons, with only a small fraction of upper layer and GABAergic neurons (Figures S1D-1H). Less than 10% of transplanted cells differentiated into astrocytes (SOX9^{+}), and none into microglia and oligodendrocytes (Figures S1I-S1K). At this stage, no KI67-expressing human cells were detected (Figure S1L). To further test the sustained stability of this cell fate, we collected snRNA-seq data at pre-transplantation, three months post-transplantation, and nine months post-transplantation, and integrated them with data obtained at twelve months after transplantation (Figure S2). This analysis showed, at the single-cell transcriptomic level, the survival, proliferation, and eventual maturation of the transplanted cells over the twelve-month period (Figure S2). Thus, transplanted human NPCs survived and differentiated into deep-layer cortical neurons, with stable proportions of CTIP2^{+}/FEZF2^{+} cells pre- and post-transplantation. We also observed that graft-derived axons (hNCAM^{+}) were enveloped by MBP^{+} cells (Figure S3A). Since no human cells become oligodendrocytes, indicated by histology (Figure S3B) and snRNA-seq (above), the MBP^{+} cells are originated from mouse oligodendrocytes. Additionally, mouse endothelial cells (Laminin^{+}) infiltrated the graft (Figure S3C), enabling blood vessels to support the grafts in a long term.

We evaluated the extension of graft-derived axons by human-specific hNCAM staining (Figure 1H), which revealed extensive axonal projections from the graft to cortical and subcortical brain regions. Semi-quantification of hNCAM^{+} axonal density in the whole brain revealed that the graft-derived axons were not only present along CST, but also in the somatosensory cortex (S1), thalamus, superior colliculus, medial vestibular nucleus, and SC (Figures S4A-S4E and S4H). In contrast, only a small number of axons followed the corpus callosum (cc) to reach the contralateral hemisphere (Figures S4F and S4H).

125 Therefore, we focused our analysis on the projection and connectivity in the ipsilateral
126 hemisphere. Robust projections were observed along the host CST from the striatum to
127 the brainstem, as revealed in sagittal sections (Figure 1I). To clearly visualize graft-
128 derived axons in the pyramidal tract, we performed tissue clearing and 3D reconstruction
129 for mCherry^{+} transplanted neurons in the brain by light-sheet microscopy (Figure 1J).
130 Fascicular mCherry^{+} axons extended through the midbrain along the pyramidal tract,
131 decussated at the medulla, and continued into the spinal cord (Figures 1J-1L and S4G).
132 Such a projection pattern of transplanted neurons (CTIP2^{+}/ FEZF2^{+}/ TBR1^{-}) resembles
133 that of endogenous corticospinal neurons.

134

135 ***Transplanted neurons synapse with host subcortical neurons with specificity***

136 Functional restoration depends on integration of transplanted neurons into the existing
137 circuits. To evaluate the global post-synaptic connectivity of transplanted neurons in the
138 adult brain and spinal cord, we developed an ESC line that expresses the anterograde
139 trans-synaptic protein mWGA-mCherry (mWmC), a mono-synaptic tracer[18], driven by the
140 synapsin1 promoter (Figure 2A). In vitro, the mWmC was only detected in neurons
141 (NeuN^{+}) but not in non-neural cells (Figure S5A). We first co-cultured mWmC/GFP neural
142 progenitor cells with wild-type neural progenitors and did not observe punctate red signal
143 in the wild-type cells (Figure S5B), indicating that mWmC is not transmitted between
144 progenitor cells. To further establish that mWmC functions as a monosynaptic tracer, we
145 cultured upstream mWmC/GFP-expressing neurons and downstream hM3Dq-mCherry–
146 labeled neurons in adjacent chambers, with mCherry labeling the cell membrane to
147 demarcate cell body (Figure S5C). Following axonal projections from the mWmC/GFP
148 neurons to the downstream neurons, punctate red signals were detected exclusively in
149 the first-order postsynaptic neurons but not in second-order neurons (Figure S5C).
150 Following transplantation, we detected mWmC signals in the host neurons, suggesting
151 that transplanted neurons formed synaptic connections with downstream host neurons
152 (Figure 2B). A substantial number of mWmC-positive host neurons were observed in the
153 S1, striatum, thalamus, subthalamic nucleus (STN), superior colliculus (SuC), pontine
154 gray (Pon G) (Figures 2C-2G). In contrast, despite extensive graft-derived axons, there
155 were few mWmC-labelled cells observed in the substantia nigra (Figure 2G). These

156 results indicate that transplanted neurons make connections with neurons in specific
157 target brain regions until their axons reach the targets rather than form stochastic
158 connections with nearby host neurons based on proximity.

159 We next mapped the connections of graft-derived axons, showing that the transplanted
160 neurons projected to and established synaptic connectivity in motor-related brain areas
161 including S1, striatum, thalamus, STN, SuC, and Pon G (Figure 2H and 2I). This is
162 strikingly similar to the endogenous targets of the motor cortex when we mapped the post-
163 synaptic connectivity by AAV-mWmC injection into the motor cortex (Figure S6A). Notably,
164 mWmC-positive cells were detected in the SC, primarily on the contralateral side (Figure
165 2J), implying that the transplanted neurons are integrated in the corticospinal circuits.
166 Remarkably, these transplanted human neurons connected with lower motor neurons
167 ($ChAT^+$) in the ventral horn of the spinal cord (Figure 2J), whereas rodent upper motor
168 neurons usually form indirect connections with lower motor neurons through interneurons
169 rather than direct connection[19-21]. To verify this distinction, we examined lower motor
170 neurons in the spinal cord following AAV-mWmC injection in intact motor cortex and found
171 no detectable mWmC signals in spinal motor neurons (Figure S6B), supporting the
172 absence of direct connections rodents.

173 At the cellular level, our immunohistochemistry results showed that the transplanted
174 neurons established connections with CTIP2+ spiny GABAergic projection neurons in the
175 striatum (Figure S7A), ($vGLUT1^+$) glutamatergic and ($GAD67^+$) GABAergic neurons in the
176 thalamus, and glutamatergic neurons in the STN, as indicated by the mCherry signal in
177 those cells (Figures S7B, S7C, and S7F). Meanwhile, mWmC was not detected in
178 dopaminergic neurons in the substantia nigra (SN) (Figure S7D). The grafted neurons
179 formed post-synaptic connections with interneurons in the SC (Figures S7E and S7F).

180

181 ***Transplanted cortical neurons make functional connections with host neurons***

182 To test if the connections between transplanted neurons and host neurons are functional,
183 we generated a DREADD/mWmC hESC line which expresses the excitatory hM3Dq
184 receptor regulated by Deschloroclozapine (DCZ) and the trans-synaptic tracer mWmC
185 (Figures 3A and S8A). This strategy allows us to simultaneously assess trans-synaptic

connections using mWmC labelling and functional synaptic connectivity via DREADD activation. Administration of DCZ (0.05mg/kg) significantly increased the expression of the activity-dependent protein FOS in transplanted neurons, indicating that DCZ treatment activated the transplanted DREADD/mWmC neurons (Figure 3B). Immunohistochemical co-staining of FOS and WGA showed that following DCZ activation of the transplanted neurons, the proportion of synaptically connected host neurons (WGA^+) expressing FOS also significantly increased, while there was no significant change in host neurons (WGA^-) without synaptic connections with the graft (Figure 3B and 3C). These data indicate that transplanted neurons form synaptic connections with host neurons and influence their activity.

To investigate whether the neural circuits regulated by transplanted neurons restore motor function in the stroke mice, we used NPCs from an inhibitory hM4Di DREADD hESC line as donors (Figure 3D and S8B-S8F). Gait analysis by TreadScan showed that cell transplantation improved motor function in stroke mice (Figures 3E and 3F). However, after DCZ administration to inhibit the transplanted neurons, the motor functions significantly declined, indicated by reduced time and frequency of the front left paws (contralateral side) touching the treadmill belt (Figures 3F and 3G). Footprint analysis of the front left paw (FL) revealed that inhibiting the transplanted neurons led to a recurrence of motor dysfunction in the previously recovered left limb (Figures 3H and 3I). Upon grafted neuron inhibition via hM4Di activation, there was a significant increase in the swing time of the left paw, while no notable changes were observed in the right paw (Figure 3J). Meanwhile, the mice stayed close to the contralateral wall after DCZ treatment (Figure 3K). To establish the specificity of the functional effects, we conducted a detailed TreadScan analysis of locomotor patterns across all four paws. We found that recovery was most pronounced in the front left paw (FL), and DCZ administration, which inhibits the transplanted neurons, resulted in a significant decrease in FL motor performance (Figure S9A). In contrast, the other three paws did not show DCZ-related changes (Figure S9B). These findings demonstrate that DCZ specifically impaired left forelimb function, consistent with our observation that transplanted cortical neurons projected to the spinal cord at the T3 level and formed synaptic connections with lower motor neurons (Figure S9C). These data suggest that the transplanted neurons form

217 functional connections with the host neurons, and the neural circuits repaired by
218 transplanted cortical neurons underline the motor function restoration.

219

220 ***Projection of transplanted cortical neurons is subtype-specific in the ischemic***
221 ***brain***

222 Transplanted cortical neurons extended axons to multiple targets, prompting a critical
223 question of how the axonal targeting is regulated in the injured adult brain. To address
224 this, we combined multiple retrograde tracing with snRNA sequencing (MRT-seq)[5] to
225 reveal the transcriptional profiles of grafted neurons projecting to specific regions. Four
226 retrograde AAVs (GFP^+), each carrying a unique barcode, were injected into the primary
227 somatosensory cortex (S1), striatum, thalamus, and medulla (MY) five weeks prior to graft
228 dissection for snRNA-seq (Figure 4A). The retro-AAV broadly labelled the L5 and L6 host
229 cortical neurons (Figure S10A), as expected. The transplanted neurons, labelled by GFP
230 (Figure 4B) and collected from three animals for snRNA-seq (Figures S10B and S10C).
231 Strikingly, the retrogradely labelled grafted neurons formed distinct clusters (Figure 4C),
232 indicating that projection-defined neuronal groups correspond to specific transcriptional
233 subtypes. Cortical projection neurons are commonly classified into four subtypes:
234 extratelencephalic (ET), intratelencephalic (IT), corticothalamic (CT), near-projecting (NP)
235 neurons[22], although snRNA-seq revealed at least 100 putative cortical neuronal
236 subclasses[23]. Alignment with a public dataset of adult human M1 cortex (Figures S10D
237 and S10E) revealed that retrogradely labelled cells partially correspond to four neuronal
238 subtypes: L5 ET, L5 IT, L6 CT, and L5/6 NP (Figures 4C and 4D). Therefore, we named
239 the grafted cortical neurons as grafted L5 intratelencephalic (G-L5 IT, striatum-projecting),
240 grafted L6 CT (G-L6 CT), grafted L5 extratelencephalic (G-L5 ET, medulla-projecting),
241 and grafted L5/6 near-projecting (G-L5/6 NP) neurons.

242 To identify the transcription profiles of G-L5 ET neurons projecting to the SC, we injected
243 retrograde AAV with GFP in the contralateral SC and retro-AAV with RFP in the ipsilateral
244 SC, both at the C7-T1 segments (Figures S10F-S10I). The host neurons labelled by AAV
245 in the intact cortex were located in L5 (Figure S10H). 97% of retrogradely labelled grafted
246 neurons projected to the contralateral SC (GFP^+) whereas only 3% to the ipsilateral side
247 (RFP^+), as indicated by snRNA-seq (Figure 4E). Over 86% of all labelled cells belonged

248 to the same neuronal cluster, and it shared a similar transcriptome with G-L5 ET (Figure
249 4F), including HCN1, KCNH1, BCL11B, SGCZ, GRIK2, and CNTN3. In particular, HCN1
250 channel-dependent membrane properties can distinguish L5 ET (human Betz cells) from
251 L5 IT neurons[24]. Betz cells are characterized by low input resistance and distinct peak
252 resonance, reflecting their large size and high expression of genes associated with the
253 HCN channel[24,25]. The projection pattern of G-L5 ET neurons in the SC is also similar to
254 that of human Betz cells (Figure S10J). To explain the relatively human-specific
255 connections in rodents, we analyzed the DEGs of synaptic assembly between human and
256 mouse corticospinal neurons. A specific combination of synaptic assembly genes,
257 including ROBO2, NRCAM, and L1CAM, was significantly higher in the G-L5 ET neurons
258 compared to mouse corticospinal neurons (Figure S10K). ROBO2, NRCAM, and L1CAM
259 are critical receptors on the growth cone to connect to lower motor neurons[26-28]. They
260 also play a vital role in commissural neurons in forming the decussation of the pyramids.

261 These data indicate substantial transcriptomic differences among the four projection
262 defined subtypes of transplanted neurons. To investigate how transcriptomic differences
263 influence the projection patterns of these neurons in the adult brain, we analyzed the
264 DEGs among transplanted neurons with distinct projection targets. Gene ontology (GO)
265 analysis of DEGs in G-L5 ET, G-L5 IT, G-L6 CT, and G-L5/6 NP neurons revealed that
266 the top GO terms of biological processes were associated with axon guidance and
267 synapse organization/transmission (Figures 4G and S10L-S10N). Among the four
268 projection-defined subtypes, each expressed distinct combinations of canonical axon
269 guidance genes, such as ROBO1, ROBO2, SLIT1, SLIT3, and EPHA3 (Figure 4H). These
270 results highlight the transcriptomic predominance of specific genes related to axonal
271 projection, explaining why transplanted neurons of one specific transcriptomic subtype
272 mainly project to the same brain region.

273

274 ***The projection pattern is regulated by transcription factors***

275 We then ask whether modifying neuronal subtypes or their corresponding transcriptional
276 codes can alter their projection pattern in the disease model. Ctip2 is an essential
277 transcriptional factor in L5 cortical neurons[29,30]. We generated a CTIP2 knockdown
278 (CTIP2-kd) hESC line and transplanted CTIP2-kd NPCs into the ischemic cortex (Figure

279 5A). Interestingly, the axons of CTIP2-kd neurons primarily projected to the amygdala
280 (Amy) through the stria terminalis (ST) in the ipsilateral hemisphere (Figures 5B and 5C),
281 with minimal projections to the subcortical regions (Figures 5B and S11A-S11C).
282 Quantification of projections showed that the projection pattern of CTIP2-kd neurons was
283 significantly different from that of wild-type neurons with more to hippocampus,
284 basolateral amygdaloid nucleus (BLA), and basomedial amygdaloid nucleus (BMA) but
285 less to subcortical regions (Figures 5D and 5E). Furthermore, robust axons from
286 transplanted CTIP2-kd neurons crossed to the contralateral cortex through the corpus
287 callosum (cc), which is rarely observed in wild-type ESC-derived neurons (Figure 5F). In
288 germline Ctip2-deficiency mice, although the L5 neurons lack robust axons along the CST,
289 they still project to subcortical regions and do not cross to the contralateral hemisphere[29].
290 The distinct projection patterns from grafted CTIP2-kd grafted neurons indicate the
291 differences in axon guidance between the self-organizing and the mature brain
292 environment.

293 To reveal how CTIP2-kd alters axonal pathfinding, we integrated the snRNA profiling of
294 control and CTIP2-kd cells and found that while their transcriptome distance is close, 76%
295 of CTIP2-kd cells were not identified as any wild-type grafted neuron subtype (Figures
296 5G and S11D), indicating modified neuronal subtypes. The CTIP2-kd neurons also lack
297 the markers of wild-type grafted neurons, such as LDB2 and FOXP1 (Figure 5H). The
298 top-10 GO terms of biological process are linked to axon guidance and connectivity
299 (Figure 5I). Among them, 61.5% of DEGs are related to axon projection (Figure S11E).
300 In particular, the RNA levels of the axonal guidance molecules normally expressed in L5
301 ET neurons, such as ROBO2 and SLIT3, were downregulated whereas EFNB1, EFNB2,
302 NRP2 were upregulated after knocking down CTIP2 (Figure 5H). ROBO2 and SLIT3 are
303 required for forming the subcortical projection while EFNB1, EFNB2, and NRP2 play
304 critical roles in guiding axons toward the amygdala and the contralateral hemisphere,
305 which may explain the altered axonal trajectory.

306 Moreover, paw-resolved grid-walking and TreadScan analysis revealed that knockdown
307 of a single transcription factor CTIP2 in transplanted cortical neurons led to strikingly
308 divergent recovery profiles (Figure S11F and S11G). Mice receiving normal
309 $CTIP2^{+}/FEZF2^{+}$ neurons showed recovery predominantly in the contralateral forelimb

310 (Figure S11F and S11H), whereas mice transplanted with CTIP2-KD neurons showed
311 recovery largely confined to the ipsilateral hindlimb (Figure S11F-S11I). Notably, these
312 behavioral outcomes are consistent with the anatomical projections of the transplanted
313 neurons within the CNS, i.e., the CTIP2-kd neurons projected to the contralateral cortex
314 to restore the corresponding functions. Hence, modification of the transcriptome by
315 altering a single transcription factor such as CTIP2 changes the axonal trajectory,
316 highlighting the requirement of a special code for the same neuronal type to navigate in
317 the mature brain.

318

319 ***Grafted neuronal subtypes carry unique transcriptional codes for axonal projection***

320 The above analysis revealed the match between the transplanted cortical neuronal
321 subtypes and the expected projection targets, raising the intriguing question of how
322 hPSC-derived neurons navigate and establish connectivity within the disorganized
323 environment of the injured brain, in contrast to the self-organizing processes during
324 development. We first evaluated the maturation state of the grafted neurons by comparing
325 them with human cortical neurons at different stages (Figure 6A)[24,31]. The clusters of
326 grafted neurons predominantly overlap with adult deep-layer cortical neuronal types
327 (Figure S12A), while fewer clusters overlap with postnatal neurons (Figure S12B). The
328 similarity was further validated by pseudotime analysis (Figures S12C-S12F). Our data
329 indicate that the four subtypes of 12-month grafted human neurons transcriptomically
330 resemble the corresponding subtypes of adult human cortical neurons in the M1 (Figure
331 3A). Both G-L5 ET and H-L5 ET neurons possess significantly higher expression levels
332 of ROBO2, PTPRM, and SEMA3D (Figures 6A and S12G), which likely facilitate the
333 formation and maintenance of corticospinal connections with spinal motor neurons[24,32].
334 Interestingly, several axon guidance molecules, including DRAXIN, UNC5C, FLRT2, and
335 NEO1, are more highly expressed in grafted corticospinal neurons compared to
336 endogenous human neurons (Figure S12G). These molecules are associated with axonal
337 repulsion, suggesting that stronger repulsion-mediated pruning may be essential for
338 directing axons along correct trajectories in the adult brain, which is also observed in L5
339 IT, L6 CT, and L5/6 NP neurons (Figure 6A). This may help explain why transplanted

340 neurons, although closely mimicking endogenous neurons in function, often fail to extend
341 their axons to appropriate target regions.

342 We next sought to identify the transcriptional code for each of the subtypes that establish
343 projections to the intended target regions (on-target), as opposed to those that merely
344 exhibit transcriptomic profiles resembling their cortical counterparts without appropriate
345 targeting (off-target), by comparing the transcriptomic differences between projection-
346 defined subtypes and their human counterparts. A set of 100 genes was calculated from
347 all genes using the "SelectKBest" method with the "f_classif" statistical test to define
348 grafted neurons in each subtype and further refined using L1-regularized logistic
349 regression and cross-validated by Bayesian Additive regression trees to obtain a code
350 with minimal numbers of genes (Figure 6B). Although the gene expression profiles of one
351 specific neuronal subtype are largely overlapping, our results demonstrate that differential
352 expressions of several selected genes is sufficient as markers to distinguish on-target
353 neurons from off-target neurons, serving as a form of transcriptional code for grafted
354 neurons (Figures 6C and 6D). Across the four neuronal subtypes, these gene
355 combinations exhibit distinct variations, suggesting the subtype specificity. Notably, most
356 of these genes are implicated in axon guidance and synapse organization, including
357 GPHN, KALRN, PTPRD, DSCAM, NRXN1, NRXN3, GRIA2, ANK2, NEGR1, NRG3,
358 LRRTM4, LRRC7, MEG3, CADM2, DLG2, and CNTNAP2 (Figure 6C).

359 To validate our formulation, we analyzed the neuronal subtypes in the cortical organoids
360 transplanted into the mouse S1 cortex[13] by integrating the snRNA-seq reference dataset
361 (Figure 6E). According to our transcriptional code-based identification, the neurons in the
362 transplanted cortical organoid comprised of 0.34% G-L5 ET, 0.20% G-L6 CT, 23.66% G-
363 L5/6 NP, and 14.36% G-L5 IT on-target neurons (Figure 6F). Indeed, the transplanted
364 (organoid) neurons project predominantly to the ipsilateral cortical and striatal regions but
365 rarely to the pyramidal tract and the ventrolateral/ventromedial thalamic nucleus[13],
366 supporting the accuracy of our model. Similarly, our codes reveal the lack of IT, ET, CT,
367 and NP subtypes in the CTIP2-kd neurons (Figure S12H), consistent with the lack of
368 ipsilateral hemisphere projections observed anatomically. Our findings show the critical
369 role of specific axon guidance profiles in identifying the neuronal subtypes. These

370 transcriptomes, while similar to those of the corresponding adult human neuronal
371 subtypes, exhibit unique features in combination and/or expression levels, serving as
372 transcriptional codes for the grafted neurons to find their targets in the adult CNS.

373

374 **DISCUSSION**

375 Defining if and how the transplanted neurons find and make functional connections with
376 their targets in the adult brain will enable us to develop effective strategies for and predict
377 the outcome of cell therapy. We established the correspondences between projection
378 targets and transplanted neuronal subtypes and identified the transcriptional code for
379 specific axonal guidance and synapse assembly in the mature brain with machine
380 learning-based regression analysis. These transcriptional codes associate transplanted
381 neuronal identity with their projection patterns. This is further supported by findings that
382 changes in neuronal identity induced by transcription factors such as CTIP2 result in
383 profound alterations in axonal projections and target recognition, suggesting that the
384 projection directions of transplanted neurons in the mature brain can be modulated
385 through transcription factor regulation. The circuits reconnected by the transplanted
386 human cortical neurons are specific and functional, as indicated by the mono-synaptic
387 anterograde tracing and activity-dependent FOS expression in the target neurons,
388 corresponding to motor behavioural recovery of the stroke mice. These transcriptome
389 profiles serve as tags to identify the complex guidance combinations, setting the
390 foundation for developing specific cell types for circuit repair.

391 It has been demonstrated that transplanted neurons form functional connections with host
392 neurons, contributing to the therapeutic effects in animal models of neurological
393 diseases[13,33-36]. The premise for choosing specific types of neuronal cells for
394 transplantation is based on the information we have learned in developing animal models,
395 i.e., a developing neuron finding its targets is largely determined by its specific
396 transcriptiome[6,37-39]. However, the environment of the brain undergoes substantial
397 modification after maturation, which alters the organization patterns of projections and
398 connectivity. Hence, the axonal projection of grafted neurons to their long-distance targets
399 is usually insufficient[2,3], or establishes inappropriate connections[40]. It is thus desirable to
400 identify the intrinsic properties or transcriptional codes of the transplantable neuronal cells

401 to achieve high-fidelity circuit integration in the adult brain. Hence, we identified the
402 specific combinations of axonal guidance and synapse organization gene profiles or
403 codes for each cortical neuronal subtype. Notably, transplanted neurons exhibited a
404 pronounced upregulation of repulsive guidance cues compared to endogenous neurons[24].
405 This differential expression pattern suggests the special balance between attractive and
406 repulsive guidance signals required for axonal navigation in the adult brain. The drastic
407 change in projection patterns by the grafted cells with CTIP2-kd highlights the regulatable
408 properties of the grafted neurons in pathfinding and circuit integration even in the adult
409 brain. And that circuit rewiring shifts functional contribution precisely from the ipsilateral
410 forelimb to contralateral hindlamb. Indeed, the corticospinal neuronal subtype in our
411 transplanted cells project axons via the pyramidal tract, cross over to the contralateral
412 side at the medulla level, and reconnect with the spinal motor neurons, which corresponds
413 to the motor behavioral recovery of the stroke mice. A striking feature of such connections
414 is direct synaptic connection between the human cortical motor neurons and the mouse
415 spinal motor neurons, a property in primates, besides indirect synapses through
416 interneurons, a characteristic in rodents. Such a phenomenon again highlights the critical
417 role of the specific transcriptional code of the grafted neurons in circuit integration. Thus,
418 the transcriptome of the transplanted cortical neuron subtypes may serve as identity tags
419 to predict their projections and connectivity, providing a guideline for selecting appropriate
420 neuronal cell types for targeted circuit reconstruction.
421

422 ***Limitations of the study***

423 The high-fidelity circuit reconstruction through transplanted neurons is influenced by
424 numerous factors. Our study revealed the roles of transcriptional codes of the major
425 cortical neuronal subtypes in pathfinding and synaptic assembly in the mature brain.
426 Analysis of additional neuronal types in other model systems will help determine if it is a
427 general principle. The similarity to as well as the difference from their endogenous
428 counterparts suggests the potential impact of the environmental signals in modulating the
429 transcription of the grafted cells, which warrants investigation.
430

431 **RESOURCE AVAILABILITY**

Microscopy data reported in this paper will be shared by the lead contact upon request.

Any additional information required to reanalyze the data reported in this paper is available from the lead contact upon request.

Lead contact

Requests for further information and resources should be directed to and will be fulfilled by the lead contact, Su-Chun Zhang (suchunz@sbpdiscovery.org).

Materials availability

Neural transplantation cocktail generated in this study will be made available on request, but we may require a payment and/or a completed materials transfer agreement if there is potential for commercial application.

Data and code availability

The snRNA-seq datasets and machine learning code are available at the Dryad with accession number 4j0zpc8qd (Dataset DOI: 10.5061/dryad.4j0zpc8qd). Allen Human Motor Cortex Atlas is from the Allen Brain Atlas Data Portal (http://help.brain-map.org/display/devmouse/API). Any additional information required to reanalyze the data reported in this paper is available from the lead contact upon request.

ACKNOWLEDGMENTS

These studies were supported in part by a Duke/Duke-NUS Pilot grant, National Medical Research Council of Singapore (MOH-000207, MOH-000212), Open Fund-Young Individual Research Grant (OFYIRG23jan-0031), and Khoo Postdoctoral Fellowship Award (Duke-NUS-KPFA/2021/0047). We thank Qiang Yuan, Ye Sing Tan, Xianfeng Tian, Chung Hock Lee, and Mynn Michele Dy Varela for dedicated technical assistance.

AUTHOR CONTRIBUTIONS

Conception and design of work, SC.Z., and ZF.W.; stroke model, ZF.W., DY.Z., and F. Y; cell transplantation, ZF.W., DY.Z., and F. Y; cell culture, ZF.W., DY.Z., and F. Y; animal breeding, ZF.W. and DY.Z.; lentivirus production, ZF.W.; cell line generation: ZF.W. and P.J.K.; electrophysiology, SM.C.; data collection, ZF.W. and DY.Z.; data analysis and interpretation, ZF.W., DY.Z., and SC.Z.; drafting the article, ZF.W. and SC.Z..

DECLARATION OF INTERESTS

The authors declare no competing interests.

463 **REFERENCES**

464 1. Espuny-Camacho, I., Michelsen, K.A., Gall, D., Linaro, D., Hasche, A., Bonnefont, J., Bali, C., Orduz,
465 D., Bilheu, A., Herpoel, A., et al. (2013). Pyramidal neurons derived from human pluripotent stem
466 cells integrate efficiently into mouse brain circuits in vivo. Neuron *77*, 440-456.
467 10.1016/j.neuron.2012.12.011.
468 2. Kitahara, T., Sakaguchi, H., Morizane, A., Kikuchi, T., Miyamoto, S., and Takahashi, J. (2020). Axonal
469 Extensions along Corticospinal Tracts from Transplanted Human Cerebral Organoids. Stem Cell
470 Reports *15*, 467-481. 10.1016/j.stemcr.2020.06.016.
471 3. Cao, S.Y., Yang, D., Huang, Z.Q., Lin, Y.H., Wu, H.Y., Chang, L., Luo, C.X., Xu, Y., Liu, Y., and Zhu, D.Y.
472 (2023). Cerebral organoids transplantation repairs infarcted cortex and restores impaired
473 function after stroke. NPJ Regen Med *8*, 27. 10.1038/s41536-023-00301-7.
474 4. Kebschull, J.M., Garcia da Silva, P., Reid, A.P., Peikon, I.D., Albeanu, D.F., and Zador, A.M. (2016).
475 High-Throughput Mapping of Single-Neuron Projections by Sequencing of Barcoded RNA. Neuron
476 *91*, 975-987. 10.1016/j.neuron.2016.07.036.
477 5. Xu, P., Peng, J., Yuan, T., Chen, Z., He, H., Wu, Z., Li, T., Li, X., Wang, L., Gao, L., et al. (2024). High-
478 throughput mapping of single-neuron projection and molecular features by retrograde barcoded
479 labeling. Elife *13*. 10.7554/eLife.85419.
480 6. Klingler, E., Tomasello, U., Prados, J., Kebschull, J.M., Contestabile, A., Galiñanes, G.L., Fièvre, S.,
481 Santinha, A., Platt, R., Huber, D., et al. (2021). Temporal controls over inter-areal cortical
482 projection neuron fate diversity. Nature *599*, 453-457. 10.1038/s41586-021-04048-3.
483 7. Van Battum, E.Y., Brignani, S., and Pasterkamp, R.J. (2015). Axon guidance proteins in neurological
484 disorders. Lancet Neurol *14*, 532-546. 10.1016/s1474-4422(14)70257-1.
485 8. Linaro, D., Vermaercke, B., Iwata, R., Ramaswamy, A., Libé-Philippot, B., Boubakar, L., Davis, B.A.,
486 Wierda, K., Davie, K., Poovathingal, S., et al. (2019). Xenotransplanted Human Cortical Neurons
487 Reveal Species-Specific Development and Functional Integration into Mouse Visual Circuits.
488 Neuron *104*, 972-986.e976. 10.1016/j.neuron.2019.10.002.
489 9. Michelsen, K.A., Acosta-Verdugo, S., Benoit-Marand, M., Espuny-Camacho, I., Gaspard, N., Saha,
490 B., Gaillard, A., and Vanderhaeghen, P. (2015). Area-specific reestablishment of damaged circuits
491 in the adult cerebral cortex by cortical neurons derived from mouse embryonic stem cells. Neuron
492 *85*, 982-997. 10.1016/j.neuron.2015.02.001.
493 10. Falkner, S., Grade, S., Dimou, L., Conzelmann, K.K., Bonhoeffer, T., Götz, M., and Hübener, M.
494 (2016). Transplanted embryonic neurons integrate into adult neocortical circuits. Nature *539*,
495 248-253. 10.1038/nature20113.
496 11. Xiong, M., Tao, Y., Gao, Q., Feng, B., Yan, W., Zhou, Y., Kotsonis, T.A., Yuan, T., You, Z., Wu, Z., et
497 al. (2021). Human Stem Cell-Derived Neurons Repair Circuits and Restore Neural Function. Cell
498 Stem Cell *28*, 112-126.e116. 10.1016/j.stem.2020.08.014.
499 12. Fiorenzano, A., Storm, P., Sozzi, E., Bruzelius, A., Corsi, S., Kajtez, J., Mudannayake, J., Nelander, J.,
500 Mattsson, B., Åkerblom, M., et al. (2024). TARGET-seq: Linking single-cell transcriptomics of
501 human dopaminergic neurons with their target specificity. Proc Natl Acad Sci U S A *121*,
502 e2410331121. 10.1073/pnas.2410331121.
503 13. Revah, O., Gore, F., Kelley, K.W., Andersen, J., Sakai, N., Chen, X., Li, M.Y., Birey, F., Yang, X., Saw,
504 N.L., et al. (2022). Maturation and circuit integration of transplanted human cortical organoids.
505 Nature *610*, 319-326. 10.1038/s41586-022-05277-w.
506 14. Tornero, D., Tsupykov, O., Granmo, M., Rodriguez, C., Grønning-Hansen, M., Thelin, J., Smozhanik,
507 E., Laterza, C., Wattananit, S., Ge, R., et al. (2017). Synaptic inputs from stroke-injured brain to
508 grafted human stem cell-derived neurons activated by sensory stimuli. Brain *140*, 692-706.
509 10.1093/brain/aww347.

15. Palma-Tortosa, S., Tornero, D., Grønning Hansen, M., Monni, E., Hajy, M., Kartsivadze, S., Aktay, S., Tsupykov, O., Parmar, M., Deisseroth, K., et al. (2020). Activity in grafted human iPS cell-derived cortical neurons integrated in stroke-injured rat brain regulates motor behavior. Proc Natl Acad Sci U S A *117*, 9094-9100. 10.1073/pnas.2000690117.
16. Rust, R., Nih, L.R., Liberale, L., Yin, H., El Amki, M., Ong, L.K., and Zlokovic, B.V. (2024). Brain repair mechanisms after cell therapy for stroke. Brain *147*, 3286-3305. 10.1093/brain/awae204.
17. Wang, Z., Zheng, D., Tan, Y.S., Yuan, Q., Yuan, F., and Zhang, S.C. (2023). Enabling Survival of Transplanted Neural Precursor Cells in the Ischemic Brain. Adv Sci (Weinh) *10*, e2302527. 10.1002/advs.202302527.
18. Tsai, N.Y., Wang, F., Toma, K., Yin, C., Takatoh, J., Pai, E.L., Wu, K., Matcham, A.C., Yin, L., Dang, E.J., et al. (2022). Trans-Seq maps a selective mammalian retinotectal synapse instructed by Nephronectin. Nat Neurosci *25*, 659-674. 10.1038/s41593-022-01068-8.
19. Lemon, R.N. (2008). Descending pathways in motor control. Annu Rev Neurosci *31*, 195-218. 10.1146/annurev.neuro.31.060407.125547.
20. Zhang, Z., Su, J., Tang, J., Chung, L., Page, J.C., Winter, C.C., Liu, Y., Kegeles, E., Conti, S., Zhang, Y., et al. (2024). Spinal projecting neurons in rostral ventromedial medulla co-regulate motor and sympathetic tone. Cell *187*, 3427-3444.e3421. 10.1016/j.cell.2024.04.022.
21. Sinopoulou, E., Rosenzweig, E.S., Conner, J.M., Gibbs, D., Weinholtz, C.A., Weber, J.L., Brock, J.H., Nout-Lomas, Y.S., Royz, E., Takashima, Y., et al. (2022). Rhesus macaque versus rat divergence in the corticospinal projectome. Neuron *110*, 2970-2983.e2974. 10.1016/j.neuron.2022.07.002.
22. Gao, L., Liu, S., Gou, L., Hu, Y., Liu, Y., Deng, L., Ma, D., Wang, H., Yang, Q., Chen, Z., et al. (2022). Single-neuron projectome of mouse prefrontal cortex. Nat Neurosci *25*, 515-529. 10.1038/s41593-022-01041-5.
23. Musall, S., Sun, X.R., Mohan, H., An, X., Gluf, S., Li, S.J., Drewes, R., Cravo, E., Lenzi, I., Yin, C., Kampa, B.M., and Churchland, A.K. (2023). Pyramidal cell types drive functionally distinct cortical activity patterns during decision-making. Nat Neurosci *26*, 495-505. 10.1038/s41593-022-01245-9.
24. Bakken, T.E., Jorstad, N.L., Hu, Q., Lake, B.B., Tian, W., Kalmbach, B.E., Crow, M., Hodge, R.D., Krienen, F.M., Sorensen, S.A., et al. (2021). Comparative cellular analysis of motor cortex in human, marmoset and mouse. Nature *598*, 111-119. 10.1038/s41586-021-03465-8.
25. Luo, Y., Shepherd, I., Li, J., Renzi, M.J., Chang, S., and Raper, J.A. (1995). A family of molecules related to collapsin in the embryonic chick nervous system. Neuron *14*, 1131-1140. 10.1016/0896-6273(95)90261-9.
26. Brose, K., Bland, K.S., Wang, K.H., Arnott, D., Henzel, W., Goodman, C.S., Tessier-Lavigne, M., and Kidd, T. (1999). Slit proteins bind Robo receptors and have an evolutionarily conserved role in repulsive axon guidance. Cell *96*, 795-806. 10.1016/s0092-8674(00)80590-5.
27. Jaworski, A., and Tessier-Lavigne, M. (2012). Autocrine/juxtaparacrine regulation of axon fasciculation by Slit-Robo signaling. Nat Neurosci *15*, 367-369. 10.1038/nn.3037.
28. Ashrafi, S., Betley, J.N., Comer, J.D., Brenner-Morton, S., Bar, V., Shimoda, Y., Watanabe, K., Peles, E., Jessell, T.M., and Kaltschmidt, J.A. (2014). Neuronal Ig/Caspr recognition promotes the formation of axoaxonic synapses in mouse spinal cord. Neuron *81*, 120-129. 10.1016/j.neuron.2013.10.060.
29. Arlotta, P., Molyneaux, B.J., Chen, J., Inoue, J., Kominami, R., and Macklis, J.D. (2005). Neuronal subtype-specific genes that control corticospinal motor neuron development in vivo. Neuron *45*, 207-221. 10.1016/j.neuron.2004.12.036.
30. Baker, A., Kalmbach, B., Morishima, M., Kim, J., Juavinett, A., Li, N., and Dembrow, N. (2018). Specialized Subpopulations of Deep-Layer Pyramidal Neurons in the Neocortex: Bridging Cellular

557 Properties to Functional Consequences. J Neurosci *38*, 5441-5455. 10.1523/jneurosci.0150-
558 18.2018.
559 31. Nano, P.R., Fazzari, E., Azizad, D., Nguyen, C.V., Wang, S., Kan, R.L., Wick, B., Haeussler, M., and
560 Bhaduri, A. (2023). A Meta-Atlas of the Developing Human Cortex Identifies Modules Driving Cell
561 Subtype Specification. bioRxiv. 10.1101/2023.09.12.557406.
562 32. Jaworski, A., Long, H., and Tessier-Lavigne, M. (2010). Collaborative and specialized functions of
563 Robo1 and Robo2 in spinal commissural axon guidance. J Neurosci *30*, 9445-9453.
564 10.1523/jneurosci.6290-09.2010.
565 33. Zheng, B., and Tuszynski, M.H. (2023). Regulation of axonal regeneration after mammalian spinal
566 cord injury. Nat Rev Mol Cell Biol *24*, 396-413. 10.1038/s41580-022-00562-y.
567 34. Parmar, M., Grealish, S., and Henchcliffe, C. (2020). The future of stem cell therapies for Parkinson
568 disease. Nat Rev Neurosci *21*, 103-115. 10.1038/s41583-019-0257-7.
569 35. Ceto, S., Sekiguchi, K.J., Takashima, Y., Nimmerjahn, A., and Tuszynski, M.H. (2020). Neural Stem
570 Cell Grafts Form Extensive Synaptic Networks that Integrate with Host Circuits after Spinal Cord
571 Injury. Cell Stem Cell *27*, 430-440.e435. 10.1016/j.stem.2020.07.007.
572 36. Steinbeck, J.A., Choi, S.J., Mrejeru, A., Ganat, Y., Deisseroth, K., Sulzer, D., Mosharov, E.V., and
573 Studer, L. (2015). Optogenetics enables functional analysis of human embryonic stem cell-derived
574 grafts in a Parkinson's disease model. Nat Biotechnol *33*, 204-209. 10.1038/nbt.3124.
575 37. Uzquiano, A., Kedaigle, A.J., Pigoni, M., Paulsen, B., Adiconis, X., Kim, K., Faits, T., Nagaraja, S.,
576 Antón-Bolaños, N., Gerhardinger, C., et al. (2022). Proper acquisition of cell class identity in
577 organoids allows definition of fate specification programs of the human cerebral cortex. Cell *185*,
578 3770-3788.e3727. 10.1016/j.cell.2022.09.010.
579 38. Velasco, S., Kedaigle, A.J., Simmons, S.K., Nash, A., Rocha, M., Quadrato, G., Paulsen, B., Nguyen,
580 L., Adiconis, X., Regev, A., Levin, J.Z., and Arlotta, P. (2019). Individual brain organoids reproducibly
581 form cell diversity of the human cerebral cortex. Nature *570*, 523-527. 10.1038/s41586-019-1289-
582 x.
583 39. Jgamadze, D., Lim, J.T., Zhang, Z., Harary, P.M., Germi, J., Mensah-Brown, K., Adam, C.D.,
584 Mirzakhalili, E., Singh, S., Gu, J.B., et al. (2023). Structural and functional integration of human
585 forebrain organoids with the injured adult rat visual system. Cell Stem Cell *30*, 137-152.e137.
586 10.1016/j.stem.2023.01.004.
587 40. Doerr, J., Schwarz, M.K., Wiedermann, D., Leinhaas, A., Jakobs, A., Schloen, F., Schwarz, I.,
588 Diedenhofen, M., Braun, N.C., Koch, P., et al. (2017). Whole-brain 3D mapping of human neural
589 transplant innervation. Nat Commun *8*, 14162. 10.1038/ncomms14162.

590

591

592 ## SUPPLEMENTAL INFORMATION

593 **Document S1. Figures S1–S12 and Table S1.**
594 **Video S1-S5. TreadScan tests, related to Figure 3, S9**
595

596 ## LEGENDS

597

598 **Figure 1. Transplanted human cortical neurons reconstitute the damaged cortex**
599 **and project axons to subcortical regions.**

600 (A) Cartoon outlining the differentiation of the human cortical NPCs from hESCs.

601 (B) Immunostaining for CTIP2, FEZF2, and TBR1 showing the cell population of induced
602 human cortical NPCs. Quantification on the right panel; n=5 independent samples. Scale
603 bars, 200μm.

604 (C) Experimental strategy for transplantation of human cortical NPCs in stroke mice. The
605 samples were collected at 12 months after transplantation. Scale bars, 1mm.

606 (D) Immunostaining with NeuN and STEM121(human cell marker) shows that the
607 transplanted NPCs became NeuN+ neurons and filled the ischemic cavity at 12 months
608 post-transplantation. Scale bars, 1mm.

609 (E) Immunostaining shows co-labelling of NEUN and human nuclear antigen (HNA) in
610 transplanted neurons at 12 months post-transplantation. Scale bars, 200μm.

611 (F) Immunostaining for CTIP2, FEZF2, and TBR1 on transplanted neurons at 12 months
612 post-transplantation. Scale bars, 100μm.

613 (G) Quantification for (F) shows the cell population of transplanted neurons at 12 months
614 post-transplantation. n=5 mice.

615 (H) Immunostaining for hNCAM showing axonal projections of transplanted neurons in
616 mature mouse brains.

617 (I) Magnification of (H) showing the axon projection by grafted neurons in the striatum,
618 pyramidal tract (PT) and brainstem.

619 (J to L) 3D reconstructed images of mCherry showing axon bundle derived from grafts
620 neurons in the transverse plane (J), midbrain (K), and hindbrain (L). Scale bars, 700μm
621 in (J), 200μm in (K) and (L).

622 All Data are represented as mean±SEM.

623

624 **Figure 2. Post-synaptic connectivity is mapped by anterograde tracing.**

625 (A) Cartoon illustrating the generation of the hSyn-mWmC hESC line for anterograde
626 tracing in the transplanted brain.

627 (B) Immunostaining for mCherry showed the presence of mWmC in host neurons in the
628 intact cortex adjacent to the graft. Scale bars, 100μm.

629 (C to G) Immunostaining for hNCAM and mCherry showing axons of grafted neurons
630 (hNCAM+) and mCherry labeled host neurons in ipsilateral S1 and striatum (C), thalamus
631 (D), ZI and STN (E), SuC (F), Pon G and SN (G). S1, primary somatosensory cortex. ic,
632 internal capsule. VL, ventrolateral thalamic nucleus. Rt, reticular thalamic nucleus. ZI,
633 zona incerta. STN, subthalamic nucleus. PT, pyramidal tract. SuC, superior colliculus. SN,
634 substantia nigra. Pon G, pontine grey. Scale bars, 100μm.

635 (H) Quantification of axon projection by grafted cells in mature brains. n=4-5 mice. Data
636 are represented as mean±SEM.

637 (I) Quantification of output connections of transplanted neurons (blue) and endogenous
638 corticospinal motor neurons (purple). The connectivity ratio is shown for all brain regions
639 receiving synaptic input from transplanted neurons at 12-month, compared to
640 endogenous neurons in intact M1(see Figure 7B). n=4 mice per group. Data are
641 represented as mean±SEM.

642 (J) Immunostaining showing WGA-labeled, ChAT-expressing host neurons in the spinal
643 cord. Dot plot of top marker genes. Insets are magnified on the right.

644

645 **Figure 3. Transplanted cortical neurons make functional connections with host**
646 **neurons.**

647 (A) Cartoon outlining the strategy to test the functional connections between the hESC-
648 derived neurons and host neurons by activating the grafted DREADD/mWmC-human
649 neurons with DCZ and examining the FOS expression in (WGA+) synaptically connected
650 mouse neurons.

651 (B) Immunostaining for FOS and WGA showing the expression of FOS in WGA+ neurons
652 in the presence (top) or absence (middle) of DCZ at 12-month after transplantation. The
653 bottom panels showing tissues from the animals grafted with hESC-derived neurons
654 (without DREADD) following DCZ treatment (stimulated control). Scale bars, 100μm.

655 (C) Quantification of FOS-expressing cells in the grafts (left), host brain (middle) and
656 spinal cord (right) in stroke mice, stimulated or non-stimulated. *p<0.05, **p<0.01, ***p<
657 0.005, ****p<0.001, two-way ANOVA test.

658 (D) Schematic showing the strategy to test the functional connections by inhibitory
659 DREADD (hM4Di) hESC-derived neurons at 12-month after transplantation.

660 (E) tSNE visualization of clustering of gait analysis for sham, stroke, transplanted (Tp),
661 and hM4Di activated (Tp+DCZ) mice.

662 (F) Heatmap showing difference in parameters among the sham, stroke, transplanted,
663 and transplanted with hM4Di activation group from the stroke group.

664 (G) Traces of the front left paws touching the treadmill belt in sham, stroke, Tp, and
665 Tp+DCZ groups.

666 (H) Footprints of the front paw captured in sham, stroke, Tp, and Tp+DCZ mice.

667 (I) Quantification of average print area of the contralateral front paw in the four groups.
668 n=9 mice in each condition. *p=0.0253, two-sided Student's t-test.

669 (J) Quantification of swing time of the left and right front paw before and after DCZ
670 treatment in the transplanted mice. **p=0.0031, paired two-sided Student's t-test.

671 (K) Quantification of the average distance of left wall hug before and after hM4Di
672 activation in the transplanted mice. ****p=0.0002, paired two-sided Student's t-test. All
673 Data are presented as mean±SEM.

674

675 **Figure 4. Transplanted cortical neuronal subtypes project to specific brain regions**
676 **revealed by MRT-seq.**

677 (A) Cartoon showing the strategy for multiple barcoded retrograde tracing by injecting
678 AAV into the somatosensory cortex, striatum, thalamus, and medulla of transplanted mice
679 (left).

680 (B) Immunostaining showing GFP labelling in the grafts and the neighboring host cortex.
681 The inset is magnified on the right showing NeuN and GFP-labeled cells in a layered
682 structure. Scale bars, 100μm.

683 (C) UMAP visualization of clustering of retro-AAV labeled nuclei in the grafts in (A).

684 (D) UMAP visualization showing the subtypes of transplanted cells using the human M1
685 snRNA-seq reference dataset. L5 ET, layer V extratelencephalic neurons; L5 IT, layer V
686 intratelencephalic neurons; L6 CT, layer VI corticothalamic neurons; L5/6 NP; layer V/VI
687 near-projecting neurons.

688 (E) UMAP visualization of grafted neurons retrogradely labelled from the SC. The
689 experimental strategy and UMAP visualization of transplanted neuronal subtypes are
690 shown in the left panel. UMAP visualization of transplanted neurons labelled with retro-
691 AAV is presented in the right panel. GluN, glutamatergic neurons; Astrocytes, astrocyte
692 lineage cells; L2/3, layer II or III; L5, layer V; L6, layer VI; L5/6, layer V or VI.

693 (F) Heatmap showing the top L5 ET marker expression of 50 randomly selected nuclei in
694 each subtype of transplanted neurons.

695 (G) Bar plot of enriched Gene Oncology (biology process) terms of G-L5 ET (MY) in the
696 graft dataset (C). (H) Violin plot of canonical axon guidance genes for each subtype of
697 transplanted cortical neurons in (C). S1, primary somatosensory cortex. MY, medulla. SC,
698 spinal cord.

699

700 **Figure 5. Grafted human cortical neurons alter the projection pattern when CTIP2**
701 **is knocked down.**

702 (A) Immunostaining for CTIP2 and HNA showing that reduction of CTIP2 expression in
703 CTIP2-kd (bottom) than the wild-type (top) graft. Scale bars, 100μm. Right panels
704 showing the hNCAM immunostaining on sagittal brain slices. Scale bars, 1mm.

705 (B) Immunostaining for hNCAM showing graft-derived axons of control cell line (top) and
706 Ctip2-kd cell line (bottom) in the striatum, ST, and PT in the ipsilateral hemisphere of
707 stroke mice.

(C) Immunostaining for hNCAM on the sagittal brain slices showing axon projection of the transplanted neurons derived from the control cell line (left) and CTIP2-kd cell line (right) in the stria terminalis (ST) and amygdala (Amy).

(D) Quantification of axon projection of grafted neurons in ipsilateral brain regions. n=4-5 mice in each group.

(E) Scatter plot showing brain regions with axon projection by the control cell and CTIP2-kd cell line. X: log2 fold change of axon projection, Y: -log10(p-value).

(F) Immunostaining for hNCAM on the coronal sections showing axon projection of transplanted neurons derived from the control and CTIP2-kd cell line. Right panels showed the magnification in the cc, M1. Scale bars, 1mm.

(G) UMAP visualization showing the subtypes of transplanted cells derived from control and CTIP2-kd cell lines after Seurat integration.

(H) Dot plot of top marker genes of control and CTIP2-kd neurons showing the different expression levels of axon guidance genes.

(I) Bar plot of enriched Gene Oncology – Biology Process terms between CTIP2-kd neurons versus control neurons.

All Data are represented as mean±SEM

Figure 6. Transcriptional codes for grafted cortical neurons.

(A) Heatmap showing the top marker expression in 50 randomly selected nuclei in each subtype of transplanted, adult, postnatal (8-month), fetal (6-month) human cortical neurons.

(B) Schematic showing the identification of transcriptional codes with machine learning for grafted neurons.

(C) Dot plot showing the expression levels of the minimal number of genes (transcriptional codes) to identify on-target grafted neurons in four subtypes.

(D) ROC curves showing the identification accuracy of grafted neurons in each subtype.

(E) Strategy for identification of cortical neurons from transplanted human cortical organoid (thCO).

(F) UMAP visualization (left panel) and quantification (right panel) of publicly available data of transplanted cortical neurons identified by transcriptional codes. On-, On-target grafted neurons. Off-, Off-target grafted neurons.

Figure S1. Characterization of human cortical neurons before and after transplantation.

(A) Immunostaining shows co-expression of CTIP2 and FEZF2 in human cortical neurons prior to transplantation. Scale bars, 200μm.

745 (B) Immunostaining for HNA, CTIP2, and TBR1 shows expression of deep layer marks in
746 human cortical NPCs before transplantation. Scale bars, 200μm.

747 (C) Immunostaining of DAPI and GFAP showing host astrocytes in the glial scar
748 surrounding lesion core. Scale bars, 1mm.

749 (D) Immunostaining of GFP and NeuN showing survival of GPF+ NPCs in the lesion at
750 14-day post-transplantation on the right panel. Scale bars, 1mm.

751 (E) Whole-mount fluorescence image shows that the graft (mCherry+) filled the ischemic
752 motor cortex at 12 months post transplantation. Scale bars, 1mm.

753 (F) UMAP visualization of clustering of nuclei from grafted cells.

754 (G) Feature plot showing glutamatergic neuron markers SYT1+ (left) and SATB2+ (right)
755 nuclei from (F).

756 (H) Feature plot showing deep layer neuron markers CTIP2+/FEZF2+ (left) and TBR1+
757 (right) cells.

758 (I) Feature plot showing upper layer neuron marker POU3F2+ cells.

759 (J) Feature plot showing GABAergic neuron marker GAD1+ cells.

760 (K) Feature plot showing astrocyte markers AQP4+ (left) and SLC1A3+ (right).

761 (L) Immunostaining for HNA, SOX9, and Iba1 on the brain slices showing astrocytes and
762 microglia in the grafts at 12 months post transplantation. Scale bars, 200μm.

763 (M) Feature plot showing oligodendrocyte marker OLIG1 cells.

764 (N) Feature plot showing proliferating cell marker KI67.

765

766 **Figure S2. Cell fates of transplanted neurons before and after transplantation.**

767 (A) UMAP showing the grafted cells before transplantation, 3 months post-transplantation,
768 9 months post-transplantation, and 12 months post-transplantation after Seurat
769 integration.

770 (B) Feature plots showing the expression of SOX2, NES, RBFOX3, and SATB2 of cells
771 in (A).

772 (C) UMAP showing the co-expression of SOX2, NES, RBFOX3, and SATB2 of cells in
773 (A).

774 (D) Barplots showing the proportion of cells expressing SOX2, NES, RBFOX3, and
775 STAB2 in (A).

776 (E) UMAP showing the expression of CASP9 and MKI67 of cells in (A). Bar plots on the
777 right panel showing temporal changes in the expression ratios of CASP9 and MKI67
778 following transplantation. The ratios remained largely unchanged from 3 months post-
779 transplantation onward.

780

781 **Figure S3. Myelination and vascularization in the graft.**

782 (A) Immunostaining of hNCAM and oligodendrocyte marker MBP showing graft-derived
783 axons are surrounded by mouse oligodendrocytes. The cross-sectional view is shown in
784 panel (A'), and side view in panel (A''). Yellow arrowheads indicate the relationship
785 between MBP and hNCAM signals. Scale bars, 100μm.

786 (B) Immunostaining with MBP (oligodendrocyte marker) and HNA showing no expression
787 of MBP in transplanted cells. Scale bars, 100μm.

788 (C) Immunostaining with STEM121 and endothelial marker Laminin on the brain slices of
789 12-month after transplantation, showing the mouse blood vessel endothelium grew into
790 the graft. Scale bars, 500μm. 200μm in magnification.

791

792 **Figure S4. Transplanted human cortical neurons rebuild the motor-related neural**
793 **circuits.**

794 (A) Schematic diagram showing the planes for brain sections.

795 (B to E) Immunostaining of hNCAM showing axon projections by the grafted neurons in
796 Pons and MY (B), thalamus, PT and Pons (C), striatum, ic and cp (D), and S1 and striatum
797 (E), in stroke mice 12 months post transplantation. Scale bars, 1mm. 100μm in
798 magnification.

799 (F) Immunostaining for hNCAM showing axon projections by the grafted neurons in the
800 contralateral and ipsilateral hemispheres at 12 months after transplantation. Scale bars,
801 1mm. 100μm in the magnification.

802 (G) Immunostaining for hNCAM showing graft-derived axons in the contralateral spinal
803 cord C7 (top) and T3 (bottom) at 12 months after transplantation. Scale bars, 500μm.

804 (H) Quantification of axon projection of grafted neurons in brain regions.

805 All Data are presented as mean±SEM.

806

807 **Figure S5. Validation of anterograde mono-synaptic tracer mWmC.**

808 (A) Schematic of generating GFP/mWmC cell lines to validate mWmC (left).
809 Immunostaining for NeuN, mCherry, and GFP showing that mCherry(mWmC) is only
810 detected in NeuN+ cells (right). Yellow arrowheads indicate primary neuron
811 (GFP+/mCherry+); White arrowheads indicate NeuN+ cells; open arrowheads indicate
812 NeuN- cells. Scale bars, 100μm.

813 (B) Immunostaining of NF-L, PSD95, GFP, and mCherry on neural progenitors showing
814 that the mWmC is not presented in GFP-/PSD95- neural progenitors. Dashed lines
815 indicate GFP-/PSD95- cells. Scale bars, 20μm.

816 (C) Schematic diagram showing that primary neurons (GFP+/mWmC+) project axons
817 distally to downstream neurons (hM3Dq-mCherry), validating that mWmC works as

818 monosynaptic tracer. Immunostaining of NF-L, PSD95, GFP, and mCherry on
819 downstream neurons showing no puncta red signals are detected in the second-order
820 neurons. Arrows indicate puncta red signals in the cytoplasm. (C' and C'') indicate the
821 first neurons which attach GFP+ neurites from primary neurons; C''' indicates the second-
822 order neurons. Scale bars, 20μm.

823

824 **Figure S6. Anterograde trans-synaptic tracer mWmC *in vivo*.**

825 (A) Strategy for injection of mWmC-AAV in M1c of the mouse brain. Immunostaining
826 showing mCherry (mWmC) detection in the S1, striatum, VL, Pon G and T1 (spinal cord)
827 in the mouse CNS. Scale bars, 200μm.

828 (B) Immunostaining showing mCherry (mWmC) detection in the T1, T10, and L6 (spinal
829 cord). Scale bars, 100μm.

830

831 **Figure S7. Transplanted neurons synapse with specific target neurons.**

832 (A) Immunostaining for WGA and Ctip2 showing that host medium spiny neurons (Ctip2+)
833 were labelled by WGA in the striatum at 12-mpt. Right panels show magnified view of the
834 insets in the dorsal (A') and ventral (A") striatum. Yellow arrowheads indicate
835 WGA+/Ctip2+ neurons. Scale bars, 100μm.

836 (B) Immunostaining with NeuN, WGA, and GAD67 showing that GABAergic neurons in
837 the cortex and thalamus were WGA positive. Right panels show magnification of VL and
838 S1. Yellow arrowheads indicate WGA+/GAD67+/NeuN+ cells. Scale bars, 1mm.

839 (C) Immunostaining for vGLUT1 and WGA showed that WGA labels (vGLUT1+)
840 glutamatergic neurons in the VL and STN. The magnification was shown in the right
841 panels. Yellow arrowheads indicate WGA+/vGluT1+ cells. White arrowheads indicate
842 WGA+/vGluT1- cells. Scale bars, 100μm.

843 (D) Immunostaining showing no overlap of WGA with hostdopaminergic neurons (TH+)
844 in the substantia nigra. White arrowheads indicate WGA+/ TH- cells. White arrows
845 indicate TH+/WGA- cells. Scale bars, 100μm.

846 (E) Immunostaining showing GAD67-expressing WGA-labeled host neurons in the spinal
847 cord. The insets are magnified on the right, yellow arrowheads indicate WGA+/ GAD67+
848 cells. Scale bars, 100μm.

849 (F) Quantification of the ratio of host neurons receiving output connections of grafted cells
850 in different brain regions. *$p<0.05$, **$p<0.01$, two-sided Student's t-test. Data are
851 presented as mean±SEM.

852

853 **Figure S8. Functional tests of DREADD/mWmC ESC-derived neurons.**

854 (A) Strategy for generation of hM3Dq-mCherry–mWmC-eGFP cell line (left).
855 Immunostaining showing expression of GFP and mCherry(mWmC) in 2D-cultured
856 neurons 60 (right top) and 90 (right bottom) days of induction. Scale bars, 100μm.

857 (B) The left panel shows the schematic of hM4Di (DREADD)/mWmC neurons following
858 DCZ treatment (inhibition). The middle panel shows the experimental strategy. The right
859 panel shows the calcium imaging of upstream neurons and their downstream neurons
860 following DCZ treatment. Scale bars, 100μm.

861 (C) Heatmap showing the neuronal activity of $mWmC^+$ and $mWmC^-$ neurons after DCZ
862 addition. The top panel showing the upstream neurons. The bottom panel showing the
863 downstream neurons. The right panel showing the average intensity over time.

864 (D) Heatmap showing neuronal activity of mWmC+ neurons in the striatum of mice
865 transplanted with DREADD neurons after DCZ/PBS administration. The right panel
866 showing the average intensity over time.

867 (E) Immunostaining for FOS showing the expression of FOS in host neurons in the
868 presence of DCZ at 12-month after hM4Di neural transplantation. Scale bars, 200μm.

869 (F) Quantification of FOS-expressing cells in the host brain and spinal cord in stroke mice.
870 *p<0.05, **p<0.01, Student's t-test.

871

872 **Figure S9. Association between limb movement and spinal motor neuron**
873 **connections.**

874 (A and B) Heatmap of parameters of front left paw (FL), front right paw (FR), rear left paw
875 (RL), and rear right paw (RR) in treadscan assessment of mice from transplantation (Tp),
876 transplantation with DCZ injection (Tp + DCZ; inhabitation), and Stroke group. (A) shows
877 FL. (B) shows FR, RL, and RR.

878 (C) Immunostaining for mCherry and ChAT showing the synaptic connections between
879 grafted neurons and spinal motor neurons in C7 and T2. Scale bars, 1mm.

880

881 **Figure S10. Retrograde tracing for transplanted neurons.**

882 (A) Strategy for injection of retrograde-AAV GFP with barcodes in the transplanted mouse
883 brain (left). Immunostaining for GFP and Ctip2 showing retrograde-AAV labelled layer V
884 neurons in the intact cortex (right). Scale bars, 200μm.

885 (B) Strategy for MRT-seq at 5 weeks after AAV injection. UMAP showing clusters of nuclei
886 from transplanted cells extracted from the mouse brain with barcoded retro-AAV-GFP
887 injection.

888 (C) Heatmap showing marker expression of clusters in (B).

889 (D) UMAP showing the grafted cells and human M1c snRNA-seq reference dataset after
890 Seurat integration.

891 (E) UMAP shows clustering of nuclei from grafted cells using label transferred from the
892 human M1c snRNA-seq reference dataset.

893 (F) Strategy for retrograde AAV injection in the spinal cord of transplanted stroke mice at
894 12 months after transplantation.

895 (G) Immunostaining for RFP and NeuN showing retrograde AAV-RFP-labelled axons in
896 the ipsilateral spinal cord of transplanted stroke mice. Scale bars, 1mm.

897 (H) Immunostaining of retrograde-AAV-GFP and RFP-labeled neurons in the cortex of
898 stroke mice. Scale bars, 200μm.

899 (I) Immunostaining for GFP and HNA showing the transplanted neurons were labelled by
900 retro-AAV. Scale bars, 200μm.

901 (J) Immunostaining showing axonal projection (hNCAM+) and output connection
902 (mCherry+) of grafted cells to the spinal cord (C8). DH, dorsal horn. D, dorsal funiculus.
903 VH, ventral horn. L, lateral funiculus. Scale bars, 500μm.

904 (K) Dot plot of top axon guidance/synapse assembly genes of human L5 ET versus
905 mouse L5 ET neurons. The genes expression on Grafted L5 ET neurons is represented
906 at the bottom of the plot for top feature genes.

907 (L-N) Bar plot of enriched Gene Oncology – Biology Process terms of cluster G-L5 IT (L),
908 G-L6 CT (M), and G-L5/6 NP (N) in the graft dataset.

909

910 **Figure S11. The projection pattern of transplanted CTIP2-kd neurons.**

911 (A) Schematic for brain sections of mice transplanted with CTIP2-kd human neurons.

912 (B-C) Immunostaining of hNCAM showing axon projections by the grafted CTIP2-kd
913 neurons in the striatum and PT (B), SI, ic and cp (C) at 12 months post transplantation.
914 Scale bars, 1mm.

915 (D) UMAP visualization shows the subtypes of transplanted cells derived from control and
916 CTIP2-kd cell lines after Seurat integration.

917 (E) Network of enriched Gene Oncology – Biology Process terms of cluster CTIP2-kd
918 neurons versus control neurons.

919 (F) Barplot showing the proportion of paw faults over number of steps in grid walk
920 assessment of mice with CTIP2-kd/hM4Di neurons transplantation, CTIP2-kd/hM4Di
921 neurons transplantation with DCZ injection and with WT neurons transplantation.

922 (G) UMAP showing clustering of treadscan assessments of mice from 6 groups: Sham,
923 Stroke, Tp (transplantation), Tp + DCZ (WT neurons transplantation with DCZ injection),
924 CTIP2-kd (CTIP2-kd/hM4Di neurons transplantation), CTIP2-kd + DCZ (CTIP2-kd/hM4Di
925 neurons transplantation with DCZ injection).

926 (H and I) Heatmap of parameters of front left paw (FL), front right paw (FR), rear left paw
927 (RL), and rear right paw (RR) in treadscan assessment of mice from Tp, Tp + DCZ,
928 CTIP2-kd, CTIP2-kd + DCZ and Stroke group. (H) shows FL. (I) shows FR, RL, and RR.

929

930 **Figure S12. Comparison of transplanted neurons with endogenous human neurons.**

931 (A and B) Heat maps of grafted cell clusters overlap by RNA-seq integration with human
932 adult (A) and postnatal (B) cortical cell clusters.

933 (C) UMAP plots showing the maturation trajectory in each subtype of human cortical
934 neurons from fetal, postnatal, and adult cortex.

935 (D) UMAP plots showing the transplanted, postnatal, and adult cortical neurons after
936 Seurat integration.

937 (E) Quantification of pseudotime in each subtype of cortical neurons.

938 (F) Bar plot showing the difference in pseudotime distance between grafted neurons and
939 postnatal versus adult neurons, indicating their relative similarity.

940 (G) Dot plot of canonical guidance gene expression on G-L5 ET neurons. The genes
941 expression on human L5 ET neurons (H-L5 ET) is represented on the top of the plot for
942 top feature genes.

943 (H) Dot plot showing the profiles of the minimal number of genes required to identify
944 CTIP2-kd neurons from on-target grafted neurons in four subtypes.

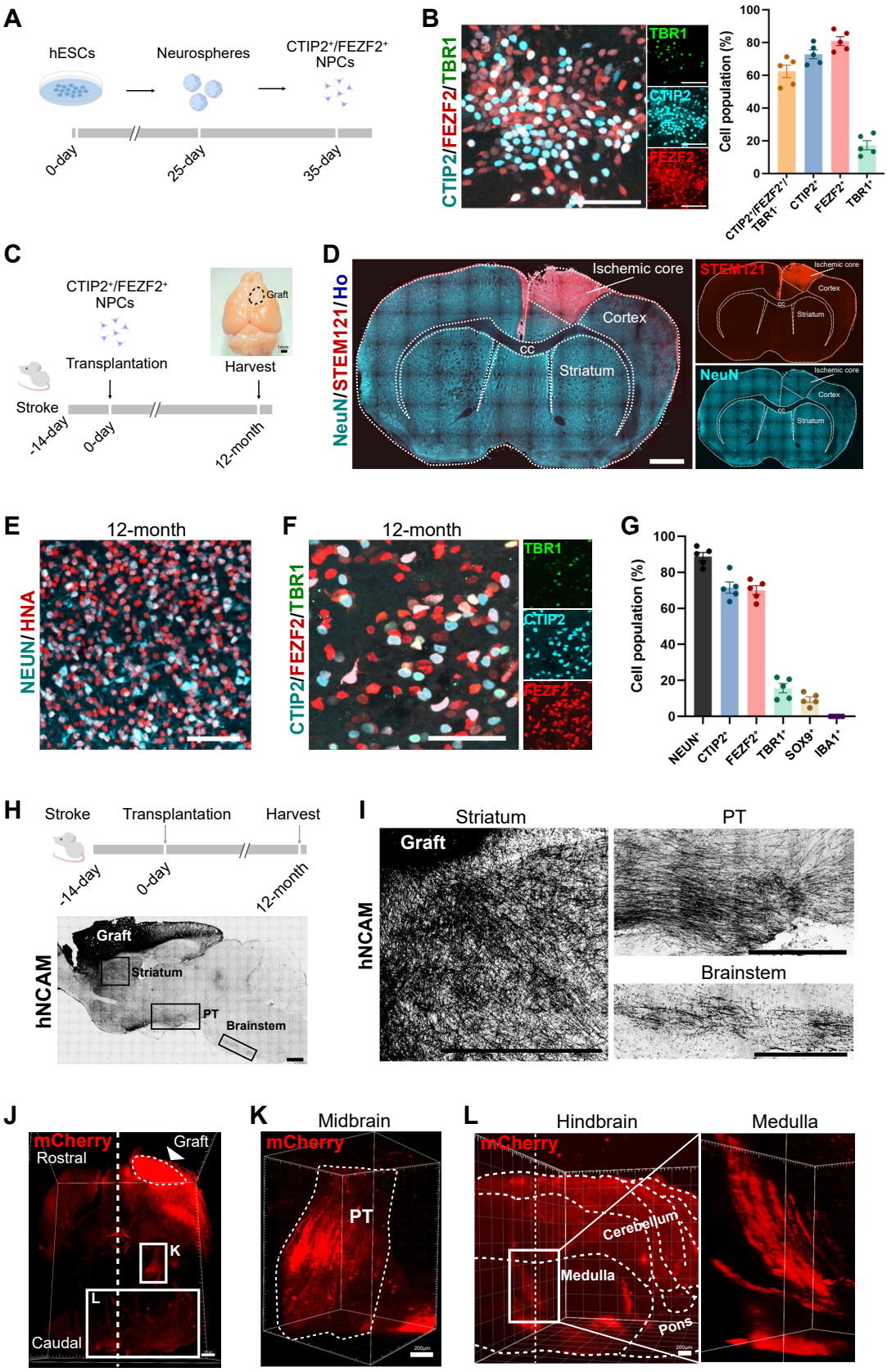

Figure 1. Transplanted human cortical neurons reconstitute the damaged cortex and project axons to subcortical regions.

(A) Cartoon outlining the differentiation of the human cortical NPCs from hESCs.
(B) Immunostaining for CTIP2, FEZF2, and TBR1 showing the cell population of induced human cortical NPCs. Quantification on the right panel; n=5 independent samples. Scale bars, 200μm.
(C) Experimental strategy for transplantation of the human cortical NPCs in stroke mice. The samples were collected at 12 months after transplantation. Scale bars, 1mm.
(D) Immunostaining with NeuN and STEM121(human cell marker) shows that the transplanted NPCs became NeuN+ neurons and filled the ischemic cavity at 12 months post-transplantation. Scale bars, 1mm.
(E) Immunostaining shows co-labelling of NEUN and human nuclear antigen (HNA) in transplanted neurons at 12 months post-transplantation. Scale bars, 200μm.
(F) Immunostaining for CTIP2, FEZF2, and TBR1 on transplanted neurons at 12 months post-transplantation. Scale bars, 100μm.
(G) Quantification for (F) shows the cell population of transplanted neurons at 12 months post-transplantation. n=5 mice.
(H) Immunostaining for hNCAM showing axonal projections of transplanted neurons in mature mouse brains.
(I) Magnification of (H) showing the axon projection by grafted neurons in the striatum, pyramidal tract (PT) and brainstem.
(J to L) 3D reconstructed images of mCherry showing axon bundle derived from grafts neurons in the transverse plane (J), midbrain (K), and hindbrain (L). Scale bars, 700μm in (J), 200μm in (K) and (L).
All Data are represented as mean±SEM.

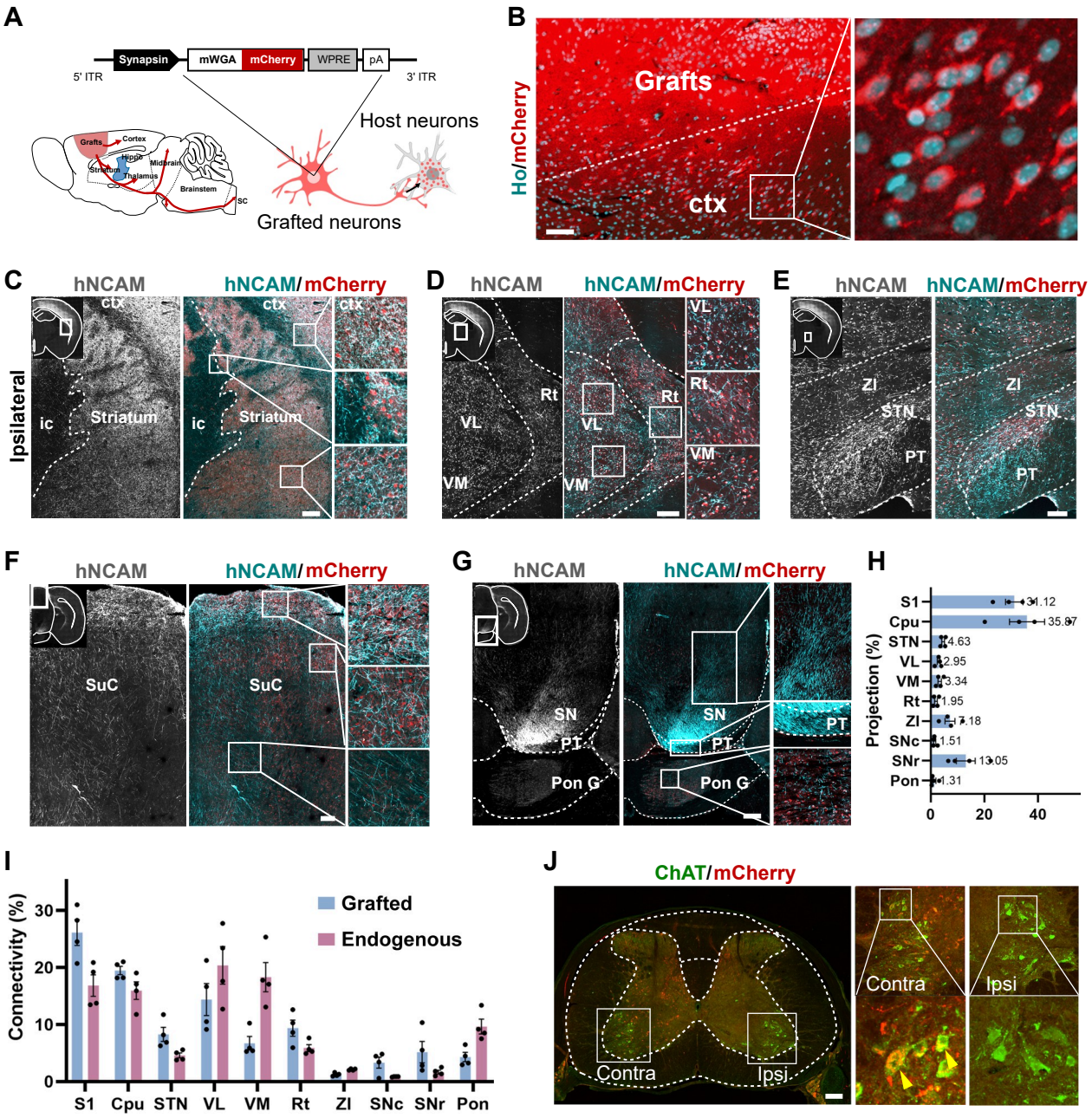

Figure 2. Post-synaptic connectivity is mapped by anterograde tracing.

(A) Cartoon illustrating the generation of the hSyn-mWmC hESC line for anterograde tracing in the transplanted brain.

(B) Immunostaining for mCherry showed the presence of mWmC in host neurons in the intact cortex adjacent to the graft. Scale bars, 100μm.

(C to G) Immunostaining for hNCAM and mCherry showing axons of grafted neurons (hNCAM+) and mCherry labeled host neurons in ipsilateral S1 and striatum (C), thalamus (D), ZI and STN (E), SuC (F), Pon G and SN (G). S1, primary somatosensory cortex. ic, internal capsule. VL, ventrolateral thalamic nucleus. Rt, reticular thalamic nucleus. ZI, zona incerta. STN, subthalamic nucleus. PT, pyramidal tract. SuC, superior colliculus. SN, substantia nigra. Pon G, pontine grey. Scale bars, 100μm.

(H) Quantification of axon projection by grafted cells in mature brains. n=4-5 mice. Data are represented as mean±SEM.

(I) Quantification of output connections of transplanted neurons (blue) and endogenous corticospinal motor neurons (purple). The connectivity ratio is shown for all brain regions receiving synaptic input from transplanted neurons at 12-month, compared to endogenous neurons in intact M1(see Figure 7B). n=4 mice per group. Data are represented as mean±SEM.

(J) Immunostaining showing WGA-labeled, ChAT-expressing host neurons in the spinal cord. Dot plot of top marker genes. Insets are magnified on the right.

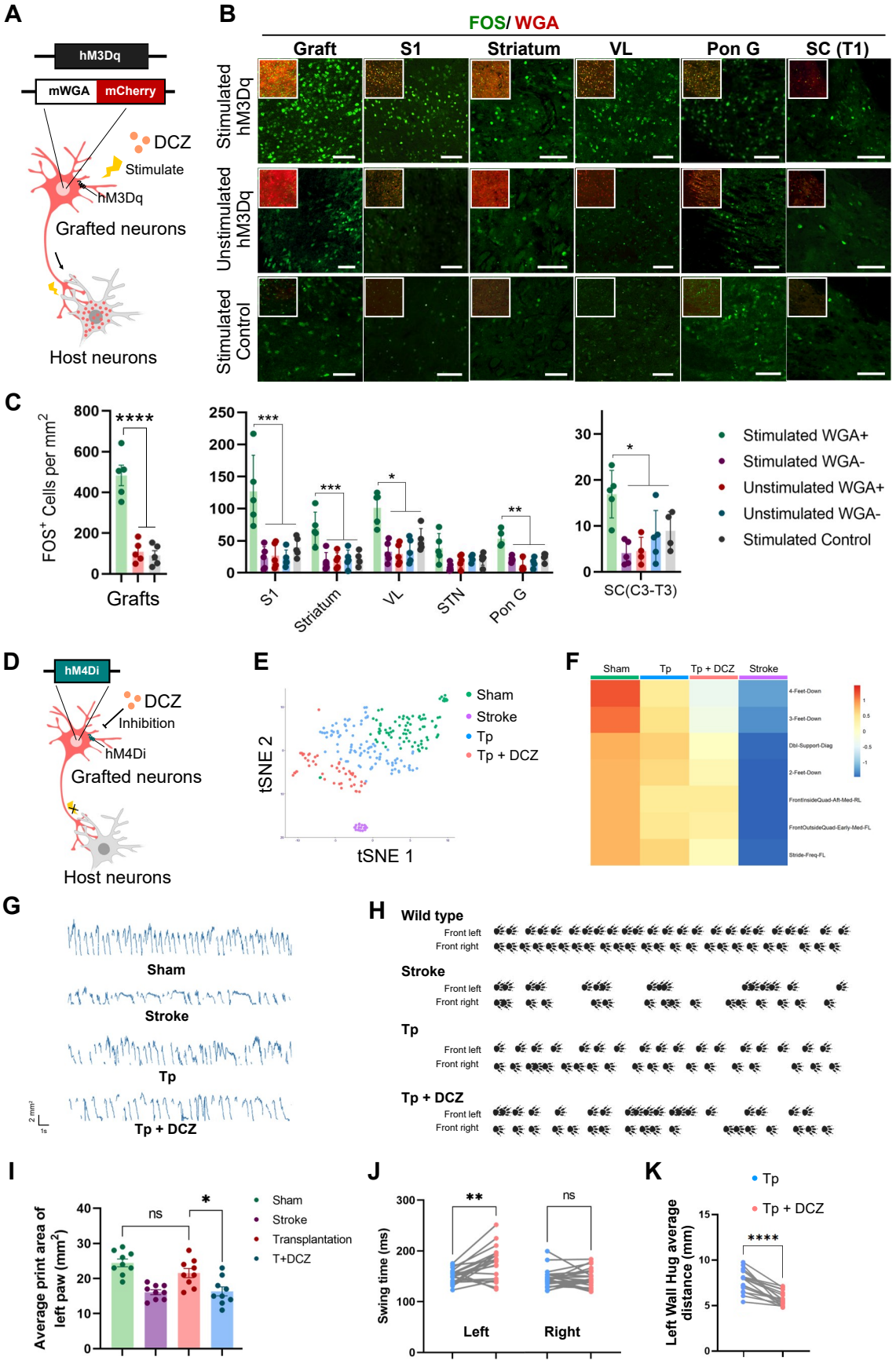

Figure 3. Transplanted cortical neurons make functional connections with host neurons.

(A) Cartoon outlining the strategy to test the functional connections between the hESC-derived neurons and host neurons by activating the grafted DREADD/ mWmC-human neurons with DCZ and examining the FOS expression in (WGA+) synaptically connected mouse neurons.

(B) Immunostaining for FOS and WGA showing the expression of FOS in WGA^+ neurons in the presence (top) or absence (middle) of DCZ at 12-month after transplantation. The bottom panels showing tissues from the animals grafted with hESC-derived neurons (without DREADD) following DCZ treatment (stimulated control). Scale bars, 100μm.

(C) Quantification of FOS-expressing cells in the grafts (left), host brain (middle) and spinal cord (right) in stroke mice, stimulated or non-stimulated. *$p<0.05$, **$p<0.01$, ***$p< 0.005$, ****$p<0.001$, two-way ANOVA test.

(D) Schematic showing the strategy to test the functional connections by inhibitory DREADD (hM4Di) hESC-derived neurons at 12-month after transplantation.

(E) tSNE visualization of clustering of gait analysis for sham, stroke, transplanted (Tp), and hM4Di activated (Tp+DCZ) mice.

(F) Heatmap showing difference in parameters among the sham, stroke, transplanted, and transplanted with hM4Di activation group from the stroke group.

(G) Traces of the front left paws touching the treadmill belt in sham, stroke, Tp, and Tp+DCZ groups.

(H) Footprints of the front paw captured in sham, stroke, Tp, and Tp+DCZ mice.

(I) Quantification of average print area of the contralateral front paw in the four groups. n=9 mice in each condition. *$p=0.0253$, two-sided Student's t-test.

(J) Quantification of swing time of the left and right front paw before and after DCZ treatment in the transplanted mice. **$p=0.0031$, paired two-sided Student's t-test.

(K) Quantification of the average distance of left wall hug before and after hM4Di activation in the transplanted mice. ****$p=0.0002$, paired two-sided Student's t-test. All Data are presented as mean±SEM.

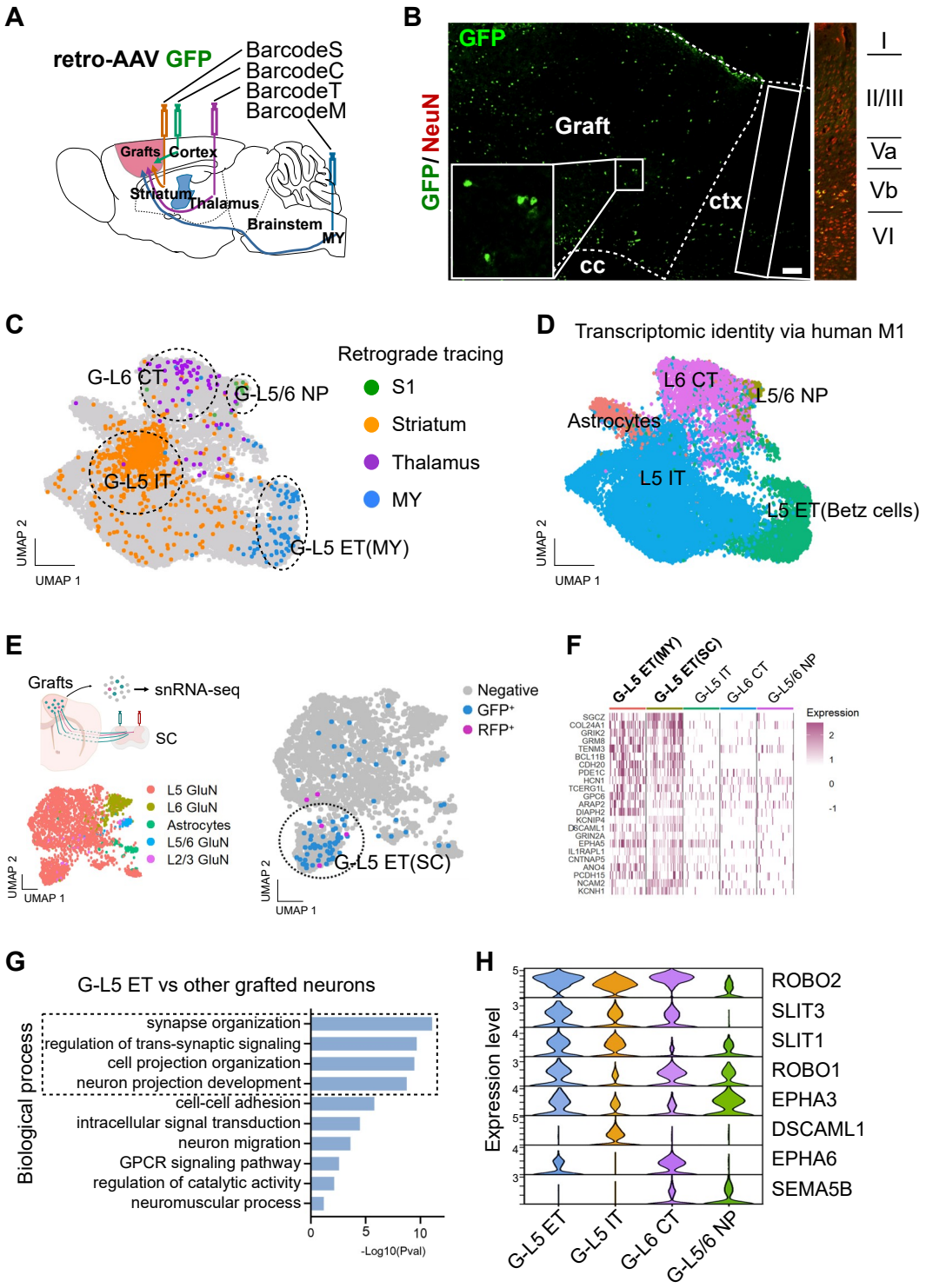

Figure 4. Transplanted cortical neuronal subtypes project to specific brain regions revealed by MRT-seq.

(A) Cartoon showing the strategy for multiple barcoded retrograde tracing by injecting AAV into the somatosensory cortex, striatum, thalamus, and medulla of transplanted mice (left).

(B) Immunostaining showing GFP labelling in the grafts and the neighboring host cortex. The inset is magnified on the right showing NeuN and GFP-labeled cells in a layered structure. Scale bars, 100μm.

(C) UMAP visualization of clustering of retro-AAV labeled nuclei in the grafts in (A).
(D) UMAP visualization showing the subtypes of transplanted cells using the human M1 snRNA-seq reference dataset. L5 ET, layer V extratelencephalic neurons; L5 IT, layer V intratelencephalic neurons; L6 CT, layer VI corticothalamic neurons; L5/6 NP; layer V/VI near-projecting neurons.
(E) UMAP visualization of grafted neurons retrogradely labelled from the SC. The experimental strategy and UMAP visualization of transplanted neuronal subtypes are shown in the left panel. UMAP visualization of transplanted neurons labelled with retro-AAV is presented in the right panel. GluN, glutamatergic neurons; Astrocytes, astrocyte lineage cells; L2/3, layer II or III; L5, layer V; L6, layer VI; L5/6, layer V or VI.
(F) Heatmap showing the top L5 ET marker expression of 50 randomly selected nuclei in each subtype of transplanted neurons.
(G) Bar plot of enriched Gene Oncology (biology process) terms of G-L5 ET (MY) in the graft dataset (C). (H) Violin plot of canonical axon guidance genes for each subtype of transplanted cortical neurons in (C). S1, primary somatosensory cortex. MY, medulla. SC, spinal cord.

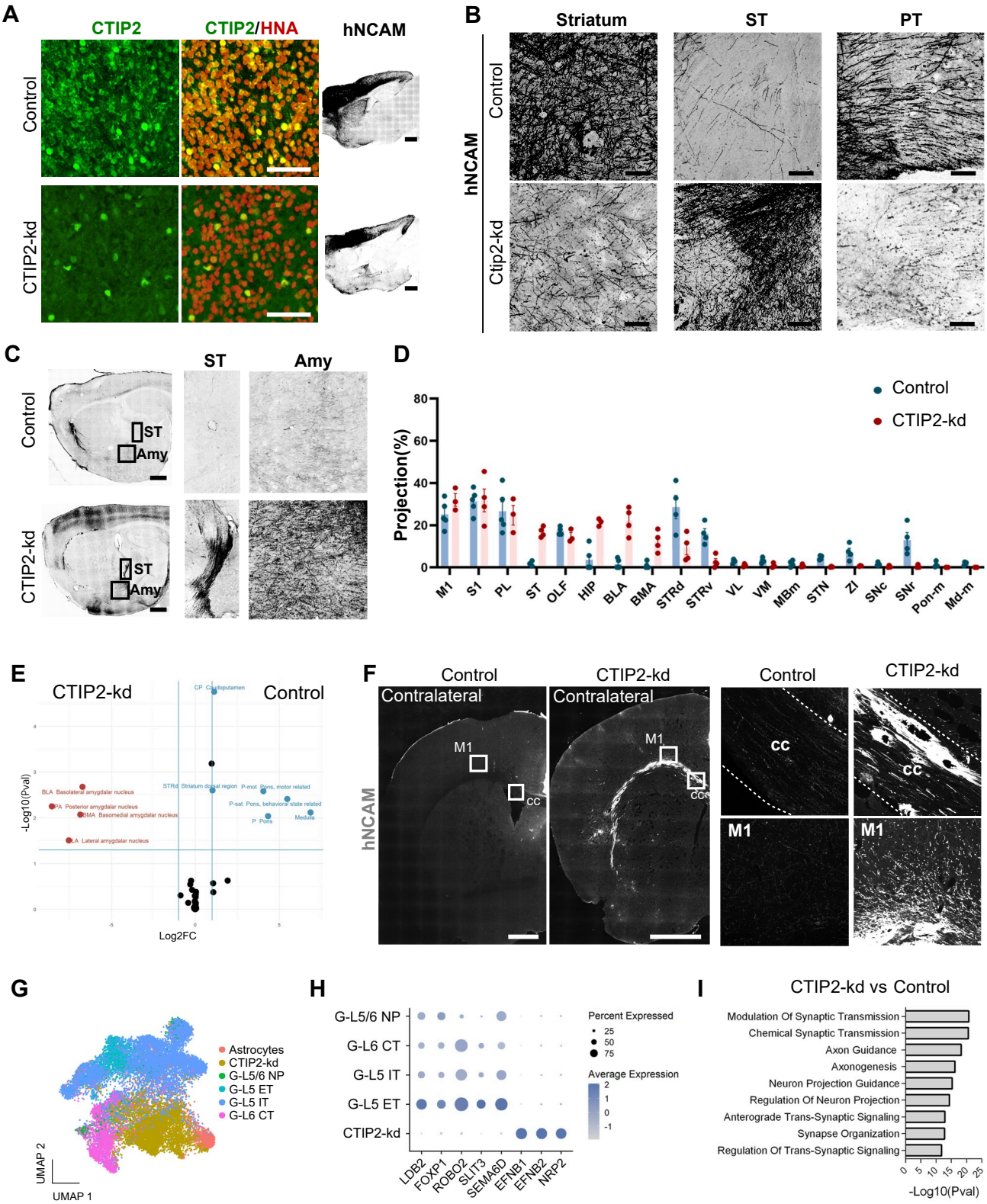

Figure 5. Grafted human cortical neurons alter the projection pattern when CTIP2 is knocked down.

(A) Immunostaining for CTIP2 and HNA showing that reduction of CTIP2 expression in CTIP2-kd (bottom) than the wild-type (top) graft. Scale bars, 100μm. Right panels showing the hNCAM immunostaining on sagittal brain slices. Scale bars, 1mm.

(B) Immunostaining for hNCAM showing graft-derived axons of control cell line (top) and Ctip2-kd cell line (bottom) in the striatum, ST, and PT in the ipsilateral hemisphere of stroke mice.
(C) Immunostaining for hNCAM on the sagittal brain slices showing axon projection of the transplanted neurons derived from the control cell line (left) and CTIP2-kd cell line (right) in the stria terminalis (ST) and amygdala (Amy).
(D) Quantification of axon projection of grafted neurons in ipsilateral brain regions. n=4-5 mice in each group.
(E) Scatter plot showing brain regions with axon projection by the control cell and CTIP2-kd cell line. X: log2 fold change of axon projection, Y: -log10(p-value).
(F) Immunostaining for hNCAM on the coronal sections showing axon projection of transplanted neurons derived from the control and CTIP2-kd cell line. Right panels showed the magnification in the cc, M1. Scale bars, 1mm.
(G) UMAP visualization showing the subtypes of transplanted cells derived from control and CTIP2-kd cell lines after Seurat integration.
(H) Dot plot of top marker genes of control and CTIP2-kd neurons showing the different expression levels of axon guidance genes.
(I) Bar plot of enriched Gene Oncology – Biology Process terms between CTIP2-kd neurons versus control neurons.
All Data are represented as mean±SEM

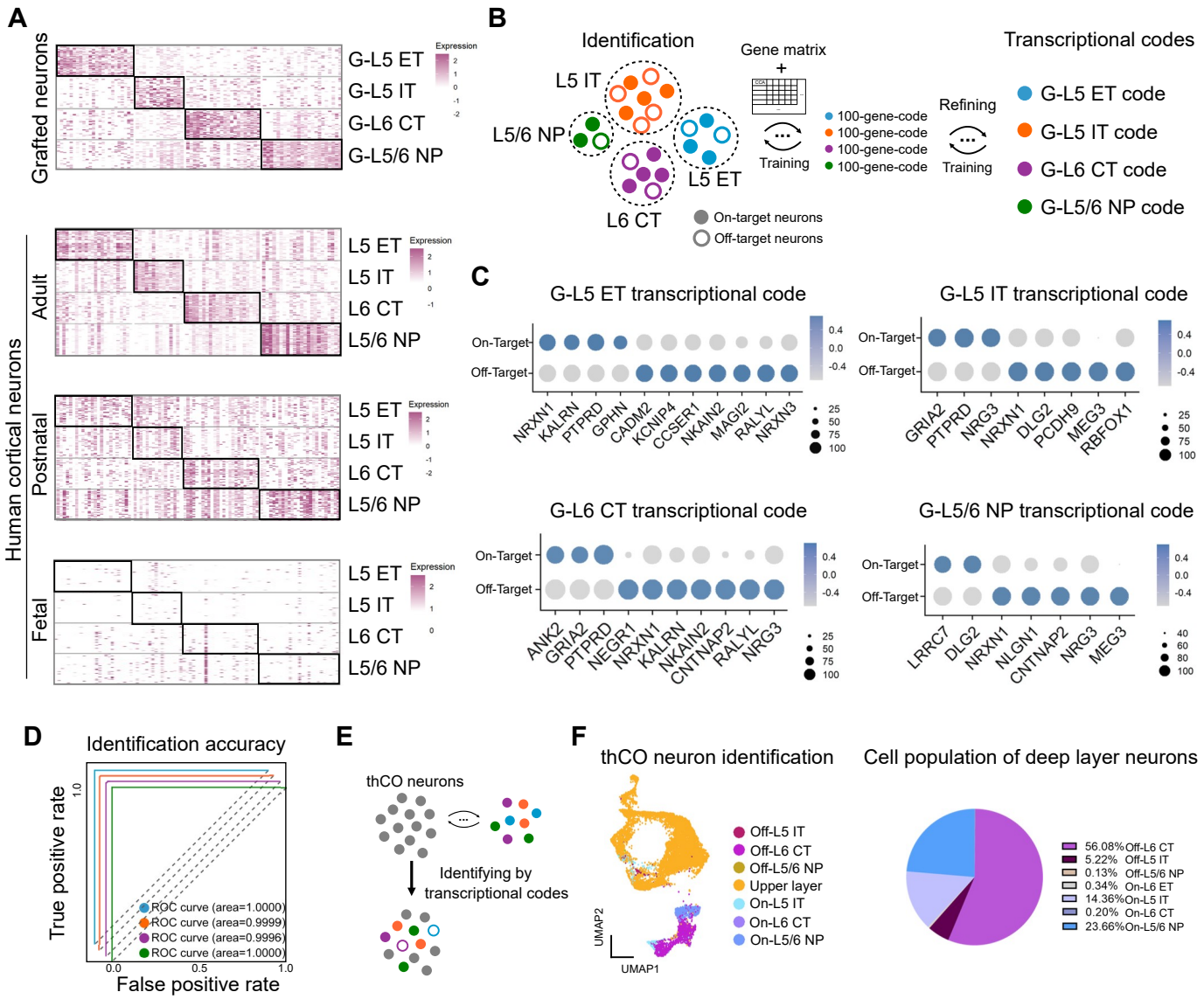

Figure 6. Transcriptional codes for grafted cortical neurons.

(A) Heatmap showing the top marker expression in 50 randomly selected nuclei in each subtype of transplanted, adult, postnatal (8-month), fetal (6-month) human cortical neurons.

(B) Schematic showing the identification of transcriptional codes with machine learning for grafted neurons.

(C) Dot plot showing the expression levels of the minimal number of genes (transcriptional codes) to identify on-target grafted neurons in four subtypes.

(D) ROC curves showing the identification accuracy of grafted neurons in each subtype.

(E) Strategy for identification of cortical neurons from transplanted human cortical organoid (thCO).

(F) UMAP visualization (left panel) and quantification (right panel) of publicly available data of transplanted cortical neurons identified by transcriptional codes. On-, On-target grafted neurons. Off-, Off-target grafted neurons.